PAPER • OPEN ACCESS

Emergence of optimal disturbances in a stratified turbulent shear flow under the stochastic forcing

View the article online for updates and enhancements.

Emergence of optimal disturbances in a stratified turbulent shear flow under the stochastic forcing

G V Zasko[1,2]**, P A Perezhogin**[2]**, A V Glazunov**[2]**, E V Mortikov**[3] **and Y M Nechepurenko**[1,2]

[1] Keldysh Institute of Applied Mathematics of the Russian Academy of Sciences, Miusskaya sq., 4, 125047, Moscow, 125047, Russia

[2] Marchuk Institute of Numerical Mathematics of the Russian Academy of Sciences, Gubkin str., 8, Moscow, 119333, Russia

[3] Research Computing Center of the Lomonosov Moscow State University, GSP-1, Leninskie Gory, 1, Moscow, 119991, Russia

E-mail: `zasko.gr@bk.ru`

Abstract. Large-scale inclined organized structures in stably stratified turbulent shear flows were revealed in the numerical simulation and indirectly confirmed by the field measurements in the stable atmospheric boundary layer. Spatial scales and forms of these structures coincide with those of the optimal disturbances of a simplified linear model. In this paper, we clarify the relation between the organized structures and the optimal disturbances, analyzing a time series of turbulent fields obtained by the RANS model with eddy viscosity/diffusivity and stochastic forcing generating the small-scale turbulence.

1. Introduction

Large-scale organized structures were revealed in numerical simulation of stably stratified turbulent shear flows close in properties to the atmospheric boundary layer (see, for example, [1], [2], [3]). These structures manifest themselves as thin inclined layers of fluid with a strong stratification (fronts) separating well-mixed regions with a weak stratification. The presence of such structures is indirectly confirmed by the field measurements in the stable atmospheric boundary layer [2], [3].

An attempt was made in [4] to explain the appearance of such organized structures in the stably stratified turbulent Couette flow by analyzing the non-modal stability of the mean turbulent flow. Within this approach, disturbances that attain a maximum amplification of their energy at finite time intervals (optimal disturbances) were found. It was shown in [4] that the optimal disturbances coincide in spatial scales and forms with the high-energy large-scale turbulent fluctuations extracted from the DNS (direct numerical simulation) results [5], [3].

However, only a few instantaneous turbulent fields from the DNS were considered in [4]. Therefore, despite a significant correlation of the optimal disturbances with the organized structures, it remains unclear whether the optimal disturbances take place in the entire dynamics of a turbulent flow, whether the organized structures appear in a nonlinear model due to the linear development of the initial optimal disturbance, and how often such events occur. This paper is devoted to these questions.

In Section 2, a simple dynamic-stochastic RANS (Reynolds Averaged Navier-Stokes) model of the emergence and development of the large-scale organized structures is proposed, which at the qualitative level has the main properties of the full DNS model. This model is used to obtain long enough time series of turbulent velocity and temperature fields. Section 3 describes the technology proposed for the analysis of the obtained time series. Conducting similar experiments with the DNS model will require significant computational resources, so we first decided to fully develop the technology of the analysis and to assess its feasibility on a computationally much simpler problem. Section 4 shows that the emergence of optimal disturbances in a nonlinear model is well described by a linear mechanism, with statistical estimates of the characteristics of this process being given. Section 5 shows that exactly the optimal disturbances are observed as organized structures. In Section 6, a universal physical mechanism for the emergence of large-scale organized structures in a turbulent flow is formulated.

2. Model of emergence and development of large-scale organized structures in the stratified turbulent Couette flow

Let us consider in Cartesian coordinates x (streamwise), y (wall-normal), z (spanwise) the motion of a viscous incompressible fluid in an infinite three-dimensional channel of half-height h: $-h < y < h$ in a gravity field. The upper wall of the channel moves with the velocity $(U_0/2, 0, 0)$, the lower one moves with the velocity $(-U_0/2, 0, 0)$, the temperatures $T_2 > T_1$ are maintained on the walls, respectively, and the velocity satisfies the no-slip condition. The fluid motion in the Boussinesq approximation is governed by the Navier-Stokes, heat transfer and continuity system of equations:

$$\frac{\partial \mathbf{v}}{\partial t} + (\mathbf{v} \cdot \nabla) \mathbf{v} + \nabla p - \frac{1}{\mathrm{Re}} \Delta \mathbf{v} - (0, \mathrm{Ri}T, 0)^T = 0,$$
$$\frac{\partial T}{\partial t} + (\mathbf{v} \cdot \nabla) T - \frac{1}{\mathrm{PrRe}} \Delta T = 0, \tag{1}$$
$$\nabla \cdot \mathbf{v} = 0,$$

where $\nabla = (\partial/\partial x, \partial/\partial y, \partial/\partial z)^T$ is the nabla operator and $\Delta = \partial^2/\partial x^2 + \partial^2/\partial y^2 + \partial^2/\partial z^2$ is the Laplace operator. Here $\mathbf{v} = (U, V, W)^T$, p and T are dimensionless components of the velocity vector (in the directions of x, y, z), the specific pressure and temperature, respectively; $\mathrm{Re} = U_0 h/\nu$, $\mathrm{Ri} = g\,(T_2 - T_1)\,h/(T_1 U_0^2)$ and $\mathrm{Pr} = \nu/\mu$ are Reynolds, Richardson and Prandtl numbers, ν is the kinematic viscosity, μ is the thermal diffusivity, g is the acceleration due to gravity.

The DNS of (1) was performed in [5], [3] in the computational domain with sizes $L_x = 12$, $L_y = 2$, $L_z = 8$ for a fixed Prandtl number $\mathrm{Pr} = 0.7$ and in a wide range of Reynolds and Richardson numbers. In this study we consider only the case of $\mathrm{Re} = 4 \cdot 10^4$, $\mathrm{Ri} = 0.03$. To compute the mean profiles of the turbulent flow, averaging (denoted by $\overline{(\cdot)}$) was made over the horizontal coordinates and time in a sufficiently large part of the model trajectory after reaching a quasi-equilibrium state by the turbulent flow. The mean values of the streamwise velocity and temperature will be further denoted by $\bar{U} = \bar{U}(y)$ and $\bar{T} = \bar{T}(y)$, respectively.

We assume that turbulent fluctuations can be separated into those $\tilde{U}'$, $\tilde{V}'$, $\tilde{W}'$, $\tilde{T}'$, $\tilde{P}'$ of a large spatial scale having the form of organized structures, and small-scale turbulent fluctuations U', V', W', T', P'. We represent the turbulent fields in the form

$$U = \bar{U} + \tilde{U}' + U', \quad V = \tilde{V}' + V', \quad W = \tilde{W}' + W', \quad T = \bar{T} + \tilde{T}' + T', \quad p = \bar{P} + \tilde{P}' + P' \tag{2}$$

and substitute (2) into (1), filtering out the small-scale turbulent fluctuations by the Reynolds

averaging. Therefore we obtain the following system of equations

$$\frac{\partial \mathbf{v}}{\partial t} + (\mathbf{v} \cdot \nabla)\,\mathbf{v} + \nabla p - \frac{1}{\mathrm{Re}}\Delta \mathbf{v} - (0, \mathrm{Ri}T, 0)^T + \overline{(\mathbf{v'} \cdot \nabla)\,\mathbf{v'}} = 0,$$

$$\frac{\partial T}{\partial t} + (\mathbf{v} \cdot \nabla)\,T - \frac{1}{\mathrm{PrRe}}\Delta T + \overline{(\mathbf{v'} \cdot \nabla)\,T'} = 0, \qquad (3)$$

$$\nabla \cdot \mathbf{v} = 0,$$

where $\mathbf{v} = (\bar{U} + \tilde{U}',\ \tilde{V}',\ \tilde{W}')^T$, $\mathbf{v'} = (U',\ V',\ W')^T$, $p = \bar{P} + \tilde{P}'$ and $T = \bar{T} + \tilde{T}'$.

The interaction of the large-scale fluctuations with the small-scale turbulence is described by the turbulent stresses $\overline{(\mathbf{v'} \cdot \nabla)\,\mathbf{v'}}$ and fluxes $\overline{(\mathbf{v'} \cdot \nabla)\,T'}$ in equation (3). Constructing a model for the development of organized structures in [4], part of the turbulent stresses characterizing the dissipative properties of a turbulent flow was parameterized by the isotropic eddy viscosity and diffusivity operators, respectively, with the coefficients $\bar{\nu}(y)$, $\bar{\mu}(y)$ depending only on the wall-normal coordinate. However, the model proposed in [4] does not represent the inherent property of turbulent flows to randomly excite large-scale fluctuations by redistributing energy from smaller to larger scales.

We suppose that the additional part of turbulent stresses can be described by the stochastic forcing $f_{\mathbf{v}} = (f_u, f_v, f_w)^T$, f_T with zero mean and variances equal to $D[(\mathbf{v'} \cdot \nabla)\,\mathbf{v'}]$ and $D[(\mathbf{v'} \cdot \nabla)\,T']$, respectively. Here $D[X]$ denotes the variance of a random field X. Then the emergence and development of the large-scale flow components appearing in the form of organized structures, can be described by the system of equations

$$\frac{\partial \mathbf{v}}{\partial t} + (\mathbf{v} \cdot \nabla)\,\mathbf{v} + \nabla p - \Delta_\nu \mathbf{v} - (0, \mathrm{Ri}T, 0)^T = f_{\mathbf{v}},$$

$$\frac{\partial T}{\partial t} + (\mathbf{v} \cdot \nabla)\,T - \Delta_\mu T = f_T, \qquad (4)$$

$$\nabla \cdot \mathbf{v} = 0.$$

Probability distributions of the stochastic forcings $f_{\mathbf{v}}$ and f_T are unknown and can be chosen only on physical grounds. We will assume that the random fields $f_{\mathbf{v}}$, f_T are independent, delta-correlated in time and horizontal coordinates, and have a normal distribution with zero mean and variance depending only on the wall-normal coordinate y.

Since the random fields $f_{\mathbf{v}}$ and f_T describe the generation of large-scale fluctuations by small-scale turbulence, it is reasonable to assume that the variance of the random field f_T is proportional to the production of temperature variance e_T:

$$e_T = \frac{1}{2}\frac{\overline{\partial T'^2}}{\partial t} = -\overline{T'V'}\frac{d\bar{T}}{dy},$$

and the total variance of $f_{\mathbf{v}}$ is proportional to the production of turbulent kinetic energy e:

$$e = \frac{1}{2}\frac{\overline{\partial (U'^2 + V'^2 + W'^2)}}{\partial t} = -\overline{U'V'}\frac{d\bar{U}}{dy}.$$

Note that the most intense generation of the small-scale turbulence occurs near the channel walls as shown in figure 1 (left).

We assume that the random field $f_{\mathbf{v}}$ is isotropic, i.e. the variance of each of its components is proportional to $e/3$, and the time scale of the correlation of random fields in the numerical model is equal to Δt (time step of the numerical model). Thus, the resulting stochastic parameterization

is as follows:

$$\overline{f_u} = \overline{f_v} = \overline{f_w} = \overline{f_T} = 0,$$
$$\overline{f_u^2} = \overline{f_v^2} = \overline{f_w^2} = \frac{2}{\Delta t} \cdot \frac{e}{3}, \qquad (5)$$
$$\overline{f_T^2} = \frac{2}{\Delta t} \cdot e_T,$$

where the power of stochastic forcing is normalized in such a way that it does not depend on Δt.

The proposed model of the stochastic forcing has shortcomings, for example, the isotropic assumption can violate close to the channel walls. However, it should be noted that the joint statistical characteristics of the part of turbulent stress tensor responsible for the interaction of small-scale turbulence with large-scale fluctuations are unknown, with the detailed DNS experiments being required. Since these are unknown, it is not possible to answer which model of the stochastic forcing is better or worse (in terms of comparison with the DNS results, which is the only reasonable quality metric) and this issue is out of the scope of the paper. Therefore, in this paper, we restrict ourselves to considering only one type of the stochastic forcing (the simplest, isotropic one).

The numerical simulation of (4) with forcing (5) was carried out in the domain with sizes $L_x = 12$, $L_y = 2$, $L_z = 8$ and the spatial resolution of $n_x \times n_y \times n_z = 48 \times 128 \times 32$ grid nodes in the directions x, y, z, respectively. Periodic boundary conditions in the directions x, z were supplied for the velocity and temperature. The parameters $e(y)$ and $e_T(y)$ of the stochastic forcing as well as the coefficients of eddy viscosity $\bar{\nu}(y)$ and diffusivity $\bar{\mu}(y)$ were taken from the DNS.

Minimum length scale reproduced by the RANS model (4) is the Kolmogorov length scale $\Delta_K = \left(\bar{\nu}^3/e\right)^{1/4}$ determined by the eddy viscosity. Figure 1 (right) shows a comparison of the Kolmogorov length scale Δ_K and the grid length scale Δ_y in the numerical realization of model (4) as a function of the wall-normal coordinate. The grid length scale Δ_y means the distance between the adjacent grid nodes. Note that a non-uniform grid along the wall-normal direction with the refinement towards the channel walls is used in the numerical model. It can be seen that in the entire domain (except for the viscous sublayer) the grid length scale is significantly smaller than the Kolmogorov length scale, i.e. the chosen spatial resolution of the model is sufficient to resolve a minimum spatial scale of equations (4).

3. Analysis of the time series
As a result of the numerical simulation of (4) with forcing (5) we get long time series consisting of $N = 5000$ instantaneous velocity and temperature fields evenly spaced with a step $\delta t \approx 0.5$. Subtracting the mean profiles of streamwise velocity $\bar{U}(y)$ and temperature $\bar{T}(y)$ produced with model (1) from each instantaneous field, a series of instantaneous fluctuation fields is obtained. These fields are expanded into a complex Fourier series in horizontal variables

$$F(x,y,z) = \sum_{k_x=-\infty}^{+\infty} \sum_{k_z=-\infty}^{+\infty} F_{k_x k_z}(y) \exp\left(\frac{2\pi \mathrm{i} k_x x}{L_x}\right) \exp\left(\frac{2\pi \mathrm{i} k_z z}{L_z}\right)$$

to extract the large-scale flow components appearing in the form of organized structures. Here k_x, k_z are streamwise and spanwise numbers of the Fourier harmonic, and i is the imaginary unit.

For a fixed Fourier harmonic with numbers (k_x, k_z), we have a time series of its amplitude which at discrete level is a rectangular complex matrix

$$\mathrm{S}_{k_x k_z} = \begin{bmatrix} \mathbf{f}_{k_x k_z}^1 & \cdots & \mathbf{f}_{k_x k_z}^N \end{bmatrix},$$
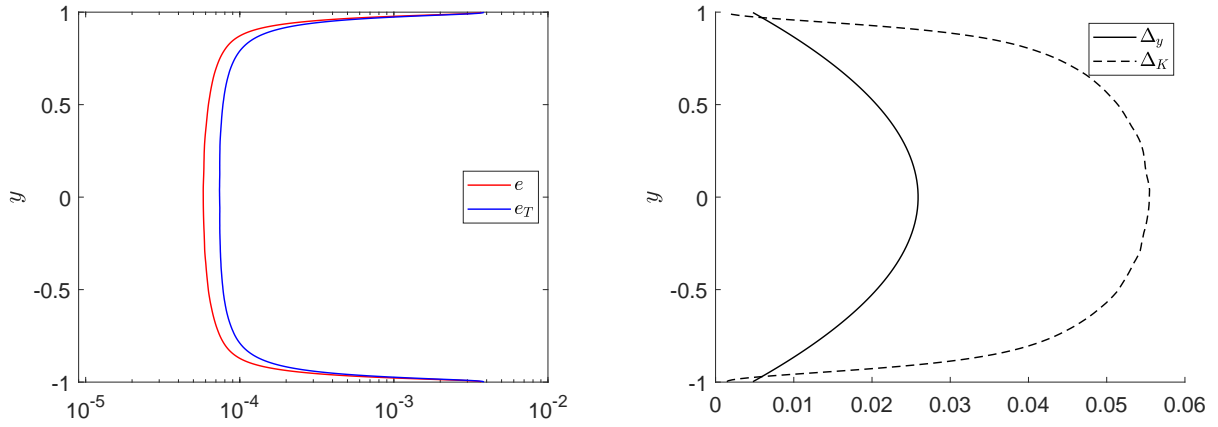
Figure 1. On the left: Parameters e (red) and e_T (blue) of the stochastic forcing (5) as a function of the wall-normal coordinate y. On the right: the Kolmogorov length scale Δ_K determined by the eddy viscosity (black dashed) and the grid length scale Δ_y (black solid) as functions of the wall-normal coordinate y.

of order $(4n_y - 1) \times N$, with the columns $\mathbf{f}_{k_x k_z}$ being the vector of amplitude values of the velocity components and temperature at the grid nodes in the wall-normal direction.

Let us define the total energy density for a fixed Fourier harmonic as

$$\mathcal{E}_{k_x k_z} = \frac{1}{2} \int_{-1}^{1} \left(|U_{k_x k_z}|^2 + |V_{k_x k_z}|^2 + |W_{k_x k_z}|^2 + \frac{\mathrm{Ri}}{d\bar{T}/dy} |T_{k_x k_z}|^2 \right) dy. \tag{6}$$

and the inner product corresponding to the discrete analog of functional (6) as

$$(a, b)_{\mathcal{E}} = \left(\mathrm{K}^2 a, b \right),$$

where K is a diagonal matrix of order $(4n_y - 1)$.

The numbers (k_x, k_z) of the Fourier harmonic correspond to a pair of wavenumbers $\alpha = 2\pi k_x / L_x$, $\gamma = 2\pi k_z / L_z$, for which we can compute the initial $\mathbf{u}_{\mathrm{opt}}^0$ and the developed $\mathbf{u}_{\mathrm{opt}}$ optimal disturbances, the time t_{opt} of the optimal disturbance growth and amplification $\Gamma_{\max}$ of its total energy density (see [4] for details).

In what follows, we study the temporal evolution of the Fourier harmonic energy

$$E_{k_x k_z}(t) = | (\mathbf{f}_{k_x k_z}(t), \mathbf{f}_{k_x k_z}(t))_{\mathcal{E}} |^2,$$

and the squared absolute values

$$P_{k_x k_z}^0(t) = | \left(\mathbf{f}_{k_x k_z}(t), \mathbf{u}_{\mathrm{opt}}^0 \right)_{\mathcal{E}} |^2, \quad P_{k_x k_z}^{\mathrm{opt}}(t) = | (\mathbf{f}_{k_x k_z}(t), \mathbf{u}_{\mathrm{opt}})_{\mathcal{E}} |^2.$$

of the Fourier harmonic amplitude projections onto the initial and the developed optimal disturbances, respectively.

Energy spectrogram, i.e. the distribution of energy over individual Fourier harmonics, can be computed for each instantaneous flow field. Averaging over all instantaneous energy spectrograms, we obtain the averaged energy spectrogram shown in figure 2 in the ranges of non-negative harmonic numbers: $0 \le k_x \le 20$, $0 \le k_z \le 20$.
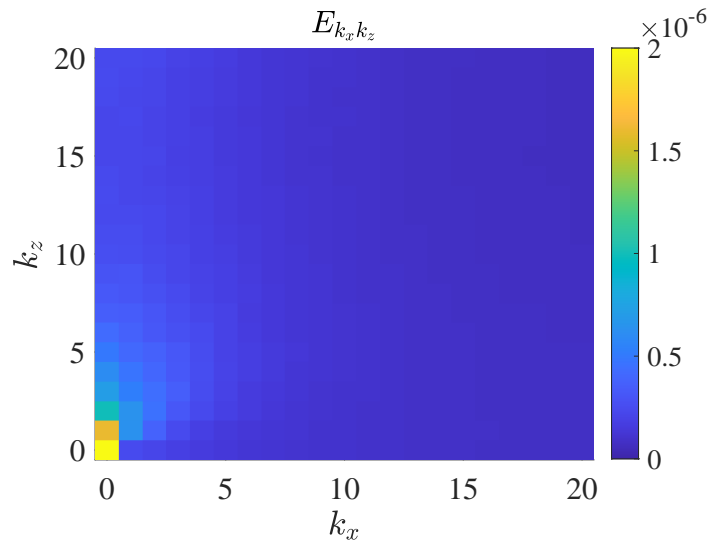
Figure 2. Averaged energy spectrogram of the instantaneous flow fields obtained from model (4) with forcing (5).

The main part of energy in figure 2 is concentrated in the large-scale Fourier harmonics. The highest energy is observed in the harmonics with zero streamwise number $(k_x, k_z) = (0, 1), (0, 2)$. Figure 2 differs from a typical spectrogram of the instantaneous fluctuation field from DNS [4], where maximum of energy is achieved at large-scale harmonics with nonzero streamwise number. The difference is apparently explained by the fact that the proposed stochastic parameterization (5) incorrectly describes the generation of the small-scale turbulence in a stably stratified turbulent flow (1).

Note that some part of energy in figure 2 falls on the harmonic with zero numbers $(k_x, k_z) = (0, 0)$, which means the difference between the mean profiles $\bar{U}(y)$ and $\bar{T}(y)$ obtained from DNS and those of obtained from model (4) with forcing (5). However, this difference is insignificant and lies mainly in the mean temperature profile.

4. Emergence of the optimal disturbances within a nonlinear model

In the linear model [4], the developed optimal disturbance $\mathbf{u}_{\mathrm{opt}}$ arises from the initial optimal disturbance $\mathbf{u}_{\mathrm{opt}}^0$ in the time t_{opt} with an amplification of energy in $\Gamma_{\max}$ times. If the optimal disturbance is governed strictly by the linear model, then

$$P_{k_x k_z}^{\mathrm{opt}}(t) = \Gamma_{\max} P_{k_x k_z}^0(t - t_{\mathrm{opt}}) \tag{7}$$

for any t. The term on the right-hand side of (7) can be interpreted as forecast of the development of the large-scale turbulent fluctuations by the linear model.

Let us check how much the temporal dynamics of the large-scale harmonics amplitudes in model (4) with forcing (5) differs from (7). It is shown in figure 3, where the dependences $P_{k_x k_z}^{\mathrm{opt}}(t)$ and $\Gamma_{\max} P_{k_x k_z}^0(t - t_{\mathrm{opt}})$ on time t are depicted for the Fourier harmonics with numbers $(k_x, k_z) = (0, 1), (1, 1)$. It can be seen that the forecast based on the linear model describes well the projection onto the developed optimal disturbance both in terms of time moments at which the peaks in energy are observed and in the magnitude of these peaks. Below we propose the statistical estimates of the parameters $t_{\mathrm{opt}}, \Gamma_{\max}$ of disturbances observed in the time series.

Estimation $\hat{t}_{\mathrm{opt}}$ of the development time can be obtained as the maximum of the cross-

correlation function

$$C_{k_x k_z}(\tau) = \frac{\text{cov}\left(P^0_{k_x k_z}(t), P^{\text{opt}}_{k_x k_z}(t+\tau)\right)}{\sqrt{D(P^0_{k_x k_z}(t)) \cdot D\left(P^{\text{opt}}_{k_x k_z}(t)\right)}} \qquad (8)$$

between the projections of the Fourier harmonic amplitudes onto the initial and the developed optimal disturbances. The cross-correlation function (8) for the large-scale harmonics with numbers $(k_x, k_z) = (0, 1), (1, 1)$ is shown in figure 4, where the value of t_{opt} produced with the linear model [4] is marked for comparison. It can be seen that $\hat{t}_{\text{opt}}$ for both cases is close to t_{opt}.

The periodicity of the cross-correlation function $C_{k_x k_z}(\tau)$ is observed for a harmonic with zero streamwise number $k_x = 0$. This might be due to the nonlinear mechanism of regeneration of large-scale streamwise streaks: the appearance of the initial optimal disturbance (streamwise rolls) leads to the developed optimal disturbance (streamwise streaks), followed by breakdown of the latter due to the secondary instability and regeneration of the former due to nonlinear interactions. This mechanism was investigated for the large-scale near-wall structures in turbulent shear flows [6], [7]. No periodicity is observed, i.e. the energy peaks randomly occur, for the harmonic with numbers $(k_x, k_z) = (1, 1)$ corresponding to the large-scale inclined structures.

Estimation $\hat{\Gamma}_{\text{max}}$ of the energy growth magnitude can be obtained as the optimal linear regression parameter

$$P^{\text{opt}}_{k_x k_z}(t) = \hat{\Gamma}_{\text{max}} P^0_{k_x k_z}(t - t_{\text{opt}}) + \varepsilon, \qquad (9)$$

directly following from (7), where ε is a random error. The scatter plots of $P^{\text{opt}}_{k_x k_z}(t)$ versus $P^0_{k_x k_z}(t - t_{\text{opt}})$ for the large-scale harmonics with numbers $(k_x, k_z) = (0, 1), (1, 1)$ are shown in figure 5 together with the optimal linear regression estimate. The statistical estimate $\hat{\Gamma}_{\text{max}}$ is rather close to Γ_{max} produced with the linear model.
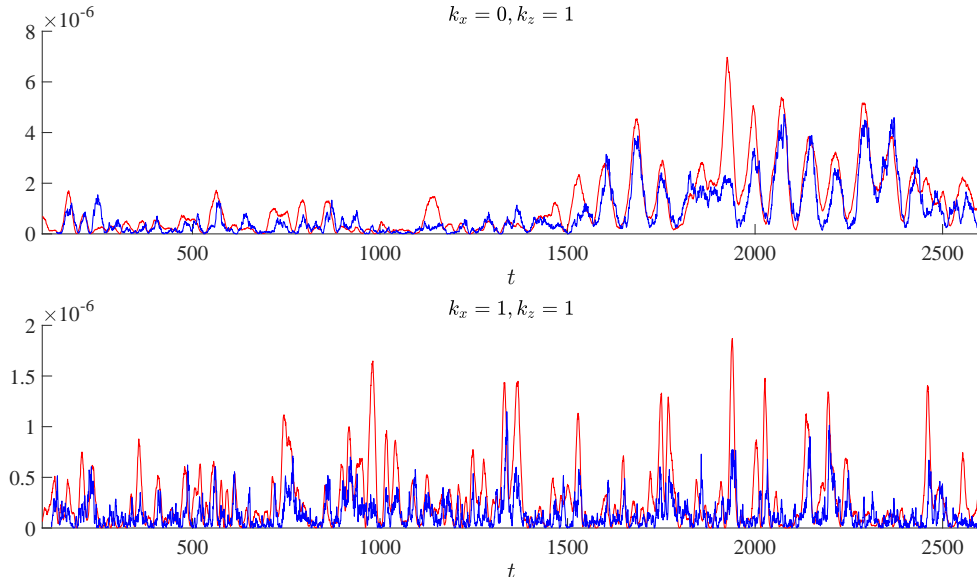
Figure 3. The time series of $P^{\text{opt}}_{k_x k_z}(t)$ (red) and its forecast $\Gamma_{\text{max}} P^0_{k_x k_z}(t - t_{\text{opt}})$ based on the linear model (blue) for the large-scale Fourier harmonics with numbers $(k_x, k_z) = (0, 1)$ (top) and $(1, 1)$ (bottom).
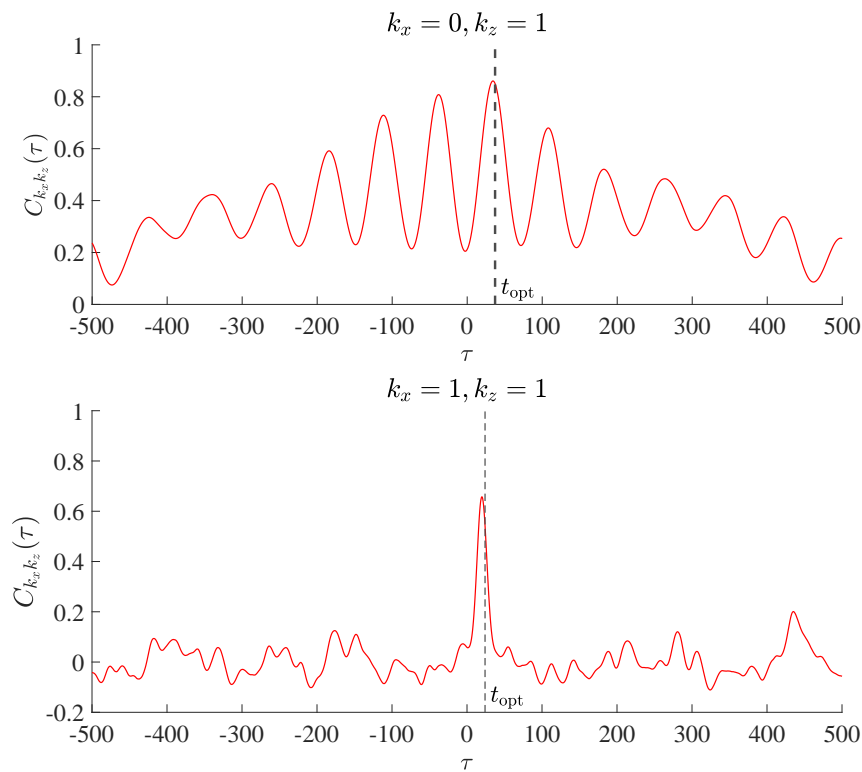
Figure 4. The cross-correlation function $C_{k_x k_z}(\tau)$ for the large-scale harmonics with numbers $(k_x, k_z) = (0, 1)$ (top) and $(1, 1)$ (bottom). The black dashed lines mark values of $t = t_{\mathrm{opt}}$ produced with the linear model [4].
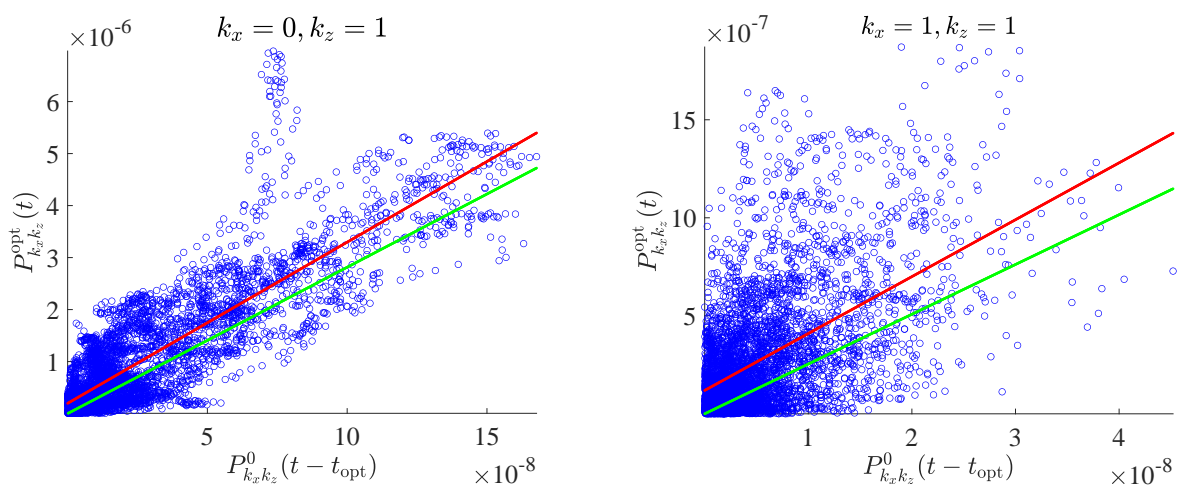
Figure 5. The scatter plots of pairs $\left(P^0_{k_x k_z}(t - t_{\mathrm{opt}}), P^{\mathrm{opt}(t)}_{k_x k_z} \right)$ (blue "○") for the large-scale harmonics with numbers $(k_x, k_z) = (0, 1)$ (left) and $(1, 1)$ (right). The estimate $\hat{\Gamma}_{\max}$ (9) and values of $\Gamma_{\max}$ produced with the linear model [4] are marked with red and green, respectively.

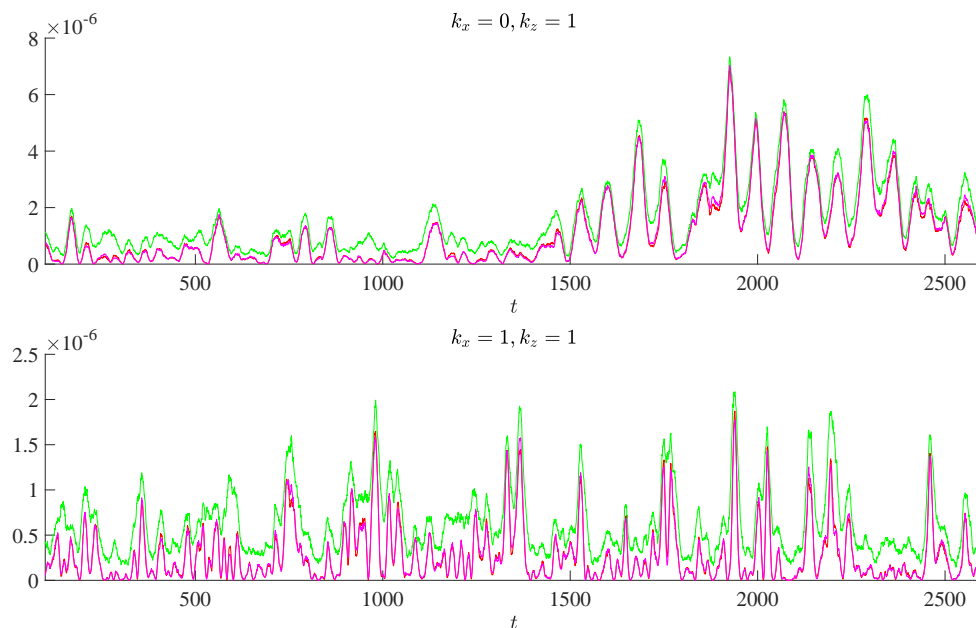## 5. Comparison of the developed optimal disturbances and the 1-st EOF

The organized structures can be extracted from the time series by the EOF analysis (EOF/PCA method, see [8], [9]). In our case, the i-th EOF is the left singular vector $\mathbf{u}_i$ of the matrix $\mathrm{KS}_{k_x k_z}$ corresponding to the i-th largest singular value σ_i. The 1-st EOF $\mathbf{u}_1$ is the spatial configuration accounting for the most of the Fourier harmonic energy in the entire time series.

In what follows, we study the squared absolute value

$$P^1_{k_x k_z}(t) = |\,(\mathbf{f}_{k_x k_z}(t), \mathbf{u}_1)_{\mathcal{E}}\,|^2$$

of the Fourier harmonic amplitude projection onto the first EOF $\mathbf{u}_1$.

The dependences of $E_{k_x k_z}(t)$, $P^{\mathrm{opt}}_{k_x k_z}(t)$ and $P^1_{k_x k_z}(t)$ on time t for the Fourier harmonics with numbers $(k_x, k_z) = (0, 1)$, $(1, 1)$ is shown in figure 6. It can be seen that the projections onto the developed optimal disturbance and the 1-st EOF almost do not differ from each other (the red line almost coincides with the pink one over the entire time series, the correlation coefficient exceeds 0.99). The time series of energy of large-scale harmonics contains sharp peaks. Both projections onto the developed optimal disturbance and the 1-st EOF are extremely large at all energy peaks.

Figure 6. The time series of $E_{k_x k_z}(t)$ (green), $P^{\mathrm{opt}}_{k_x k_z}(t)$ (red) and $P^1_{k_x k_z}(t)$ (pink) for the large-scale Fourier harmonics with numbers $(k_x, k_z) = (0, 1)$ (top), $(1, 1)$ (bottom).

Thus, it can be argued that exactly the developed optimal disturbances appear as large-scale organized structures.

6. Conclusion

To sum up, let us formulate a possible mechanism for the emergence of large-scale organized structures in a turbulent flow. As soon as disturbance appears from the small-scale turbulence that has a projection onto the initial optimal disturbance, it develops due to the mechanism described by the linear model [4]. If the value of the initial projection is large enough, then the result is the developed optimal disturbance, which manifests itself in the turbulent fluctuation

fields as organized structures. If typical values of large-scale disturbances amplitudes are small enough (i.e. nonlinearity is not decisive), then the described mechanism is able to take place.

Within the framework of the dynamic-stochastic RANS model, the statistical estimates of the development time and the energy amplification of the optimal disturbances are close to those predicted by the linear model, i.e. nonlinearity and the presence of random turbulent fluctuations are not a determining factor for the possibility of its development. To draw final conclusions, this result should be verified with the DNS.

References
[1] Glazunov A V 2014 *Izv. Atmos. Ocean. Phys.* **50** 236–245
[2] Sullivan P P, Weil J C, Patton E G, Jonker H J and Mironov D V 2016 *J. Atmos. Sci.* **73** 1815–40
[3] Glazunov A V, Mortikov E V, Barskov K V, Kadantsev E V and Zilitinkevich S S 2019 *Izv. Atmos. Ocean. Phys.* **55** 312–323
[4] Zasko G V, Glazunov A V, Mortikov E V and Nechepurenko Y M 2020 *Russ. J. Numer. Anal. Math. Model.* **35** 37–53
[5] Mortikov E V, Glazunov A V and Lykosov V N 2019 *Russ. J. Numer. Anal. Math. Model.* **34** 119–132
[6] Hamilton J M, Kim J and Waleffe F 1995 *J. Fluid Mech.* **287** 317–348
[7] Waleffe F 1997 *Phys. Fluids* **9** 883–900
[8] Preisendorfer R W and Mobley C D 1988 *Developments in Atmospheric Science* **17**
[9] Björnsson H and Venegas S A 1997 *CCGCR Report* **97** 112–134